Electron transfer behaviour of biological macromolecules towards the single-molecule level

2003 J. Phys.: Condens. Matter 15 S1873

(http://iopscience.iop.org/0953-8984/15/18/318)

INSTITUTE OF PHYSICS PUBLISHING JOURNAL OF PHYSICS: CONDENSED MATTER

J. Phys.: Condens. Matter **15** (2003) S1873–S1890 PII: S0953-8984(03)55225-0

Electron transfer behaviour of biological macromolecules towards the single-molecule level

Jingdong Zhang[1], **Mikala Grubb**[1], **Allan G Hansen**[1], **Alexander M Kuznetsov**[2], **Anja Boisen**[3], **Hainer Wackerbarth**[1] and **Jens Ulstrup**[1,4]

[1] Department of Chemistry, Building 207, Technical University of Denmark, DK-2800 Lyngby, Denmark
[2] The A N Frumkin Institute of Electrochemistry of the Russian Academy of Sciences, Leninskij Prospect 31, 117071 Moscow, Russia
[3] The Microelectronics Centre, Building 345, Technical University of Denmark, DK-2800 Lyngby, Denmark

E-mail: ju@kemi.dtu.dk

Received 25 October 2002
Published 28 April 2003
Online at stacks.iop.org/JPhysCM/15/S1873

Abstract

Redox metalloproteins immobilized on metallic surfaces in contact with aqueous biological media are important in many areas of pure and applied sciences. Redox metalloprotein films are currently being addressed by new approaches where biotechnology including modified and synthetic proteins is combined with state-of-the-art physical electrochemistry with emphasis on single-crystal, atomically planar electrode surfaces, *in situ* scanning tunnelling microscopy (STM) and other surface techniques. These approaches have brought bioelectrochemistry important steps forward towards the nanoscale and single-molecule levels.

We discuss here these advances with reference to two specific redox metalloproteins, the blue single-copper protein *Pseudomonas aeruginosa* azurin and the single-haem protein *Saccharomyces cerevisiae* yeast cytochrome *c*, and a short oligonucleotide. Both proteins can be immobilized on Au(111) by chemisorption via exposed sulfur-containing residues. Voltammetric, interfacial capacitance, x-ray photoelectron spectroscopy and microcantilever sensor data, together with *in situ* STM with single-molecule resolution, all point to a coherent view of monolayer organization with protein electron transfer (ET) function retained. *In situ* STM can also address the microscopic mechanisms for electron tunnelling through the biomolecules and offers novel notions such as coherent multi-ET between the substrate and tip via the molecular redox levels. This differs in important respects from *electrochemical* ET at a single metal/electrolyte interface. Similar data for a short oligonucleotide immobilized on Au(111) show that oligonucleotides can

[4] Author to whom any correspondence should be addressed.

be characterized with comparable detail, with novel perspectives for addressing DNA electronic conduction mechanisms and for biological screening towards the single-molecule level.

(Some figures in this article are in colour only in the electronic version)

1. Introduction

The structural organization and electron transfer (ET) functions of proteins and oligonucleotides on solid surfaces are central in new interdisciplinary areas, which combine biotechnology with physical and chemical nanoscale molecular science. Fundamental contexts are adsorption dynamics, mechanisms of long-range ET through immobilized redox metalloproteins and oligonucleotides, coupled enzyme catalysis, and oligonucleotide hybridization [1–7]. New technological nanoscale perspectives are in areas of protein–membrane interactions and drug delivery [8], biological corrosion [9], support for attached tissue cultures ('biofilms') [10], biocompatibility of metallic implants or surface chemistry of medical devices [11, 12]. To this come new *electrochemical* intermediate-sized or nanoscale systems known under appellations such as 'electrochemical nanodevices' or 'nanobioelectrochemistry' [1, 2].

Ultimate goals of emerging nanoscale bioelectrochemistry are to map and control the orientation, supramolecular organization and ET function of redox macromolecules on metallic substrates, at the monolayer and single-molecule levels. The *electrochemical* approach is here unique as the interfacial electrochemical ET signals both constitute the electrical contact to external circuits and are at the same time exceedingly sensitive monitors of the functional state of the molecules. Ultimate technological goals are to exploit organized functional redox protein and oligonucleotide monolayers to promote electronic signals (molecular ET) between molecules in solution and the electrode via the protein/oligonucleotide monolayers. Signals would also be *induced* by enzyme–substrate interactions, oligonucleotide hybridization, optical interactions or other physical interactions such as in microcantilever devices and atomic force microscopy (AFM).

Important observations on bioelectrochemical sensing toward single-molecule levels are the following.

(a) Nanoscale bioelectrochemistry is based on redox metalloproteins/metalloenzymes [3, 13], as well as synthetic oligonucleotides [14]. A central notion is protein (or oligonucleotide) *film* voltammetry, broadly developed over the last decade [3, 13, 15].
(b) A new dimension is that *de novo*, i.e. totally synthetic, pre-designed redox proteins have become available. 4-α-helix bundle proteins [16–19], have offered particular perspectives as the secondary and tertiary structures of these intermediate-size synthetic proteins can be varied systematically, enabling disclosure of new levels of detail in molecular structure–function relations. At the same time these proteins can be brought to immobilization in electrochemical environments [2, 17, 19]. This novel area of protein *design* might hold a key role in forthcoming approaches to nanoscale bioelectrochemistry.
(c) Redox metalloprotein technology has reached high levels of protein purity and characterization. This is matched by corresponding electrochemical standards. Novel bioelectrochemistry can be combined with state-of-the-art *physical* electrochemistry, involving for example single-crystal, atomically planar electrode surfaces. This is itself

novel but now established in interfacial electrochemistry of redox metalloproteins [20–22] and oligonucleotides, cf below.

Nanoscale bioelectrochemistry implies that system properties determined by the nanoscale *size* become important. The 'nanoscale' notion can apply to *different* dimensions, corresponding to molecular ladders, stripes, monolayers and single molecules [23]. Restricted dimensionality prompts the need for new *theoretical* frames. These rest on comprehensive molecular charge transfer theory in chemical, electrochemical and biological systems [24–27] but new theory is also needed, to include, for example, stochastic single-molecule features [28] or single-electron tunnelling (SET) in electrochemical and bioelectrochemical systems [29]. Other novel theory has addressed *in situ* scanning tunnelling microscopy (STM) [30, 31], and disclosed new ET *phenomena* including collective multi-ET, negative differential resistance or molecular electronics features such as molecular electrical current rectification ('the molecular diode') [32].

Interfacial (bio)electrochemical ET towards the nanoscale and single-molecule levels opens wider perspectives. In efforts towards *device* function, strategies for single-molecule component *combination* into molecular-scale electronic 'circuits', must be designed. Solid-state circuits based for example on carbon nanotubes [33], or redox-based reconfigurable (catenane- and rotaxane-based) switches [34], represent such molecular-size electronic circuit components. Electrochemically based analogues are not currently of immediate recognition, but as for fundamental nanoscale bioelectrochemistry, the *combination* of biotechnology with state-of-the-art physical electrochemistry holds options for bioelectrochemical circuit technology. This could be based, for example, on the molecular 'Lego approach' where artificial redox chains are brought to communicate electronically with the electrode surface [1, 35]. It could also involve combination of turrets [36], pits [37] or other nanoscale metallic structures with redox metalloproteins in multi-functional single-molecule biosensor arrays.

In this paper we discuss first aspects of nanoscale bioelectrochemistry in relation to other recent molecular-scale science. We then offer some notions of recent theoretical advances in electrochemical nanoscale science, with emphasis on *in situ* electrochemical STM. These observations are illustrated by recent case studies of molecular monolayer systems mapped towards nanoscale and single-molecule levels. The need for *comprehensive* experimental and theoretical efforts towards these goals is particularly noted.

2. Interfacial bioelectrochemistry towards the single-molecule level

Monolayer electrochemistry and *in situ* STM of biological macromolecules can be put in perspective by comparison with other single-molecule approaches and some theoretical notions.

2.1. Single-molecule spectroscopies and chemical reaction dynamics

Single-molecule fluorescence spectroscopy, excited state lifetimes and resonance Raman spectroscopy have provided new detail about molecular environments and stochastic distributions of single-molecule observables in time and space [38, 39]. These include time-resolved emission spectra, single-molecule vibrational fine structure and near-field Raman and resonance Raman spectra. Condensed aromatic systems, amino acids and DNA bases, DNA fragments and metalloproteins are among many different target molecules [38].

AFM adds other perspectives to *in situ* STM and nanoscale bioelectrochemistry. AFM of molecular adsorbates on solid surfaces in contact with aqueous solution does not always involve the same electrochemical potential requirements as STM. AFM has, therefore, in some

respects advanced further than STM. AFM has disclosed details of tertiary protein structure unfolding, ligand–receptor interactions and unzipping of DNA and oligonucleotides [40]. Single biomolecules in direct chemical action in aqueous buffer solution have, further, been mapped in real time by *in situ* AFM [41–44].

2.2. Comprehensive approaches to nanoscale electrochemistry and bioelectrochemistry

As noted, approaches to nanoscale bioelectrochemistry and other nanotechnology rest on a combination of physical electrochemistry and biotechnology including metalloprotein engineering and design. Direct electrochemical single-ET systems are few in number. Fluorescence decay of photo-excited cresyl violet adsorbed on indium tin oxide (ITO) could be assigned to interfacial ET to the ITO conduction band, disclosing molecular stochastic effects [45]. Ferrocenes trapped against an ITO electrode under a scanning electrochemical microscope also displayed single-molecule 0.2 pA current fluctuations [46]. Other electrochemical ET systems have shown SET and Coulomb blockade features at nanoscale electrodes [47] and gold nanoparticles [48].

In the present report a comprehensive electrochemical and biotechnological approach are combined including STM in the electrochemical *in situ* mode directly in the biological aqueous media. The electrochemical part involves voltammetry, capacitance and electrochemical impedance methodology for the biomolecular monolayers, combined with spectroscopy such as XPS, and microcantilever sensor (MCS) techniques. A crucial notion is that the nanoscale perspective requires single-crystal, atomically planar electrode surfaces. This is new in bioelectrochemistry. The biotechnological part aims at exploiting state-of-the-art preparation of protein monolayers including protein design, synthesis, assembly and wiring to the electrode. This view offers the notion of 'bioelectrochemistry at well defined surfaces', and implies that electronic and other monolayer characterization is undertaken, and a well defined environment for single-molecule *in situ* STM and functional integrity ascertained.

2.3. Some theoretical notions in single-molecule electrochemistry and in situ STM

Molecular charge transfer theory offers powerful frames in broad areas of experimental chemistry, almost comparable to many-body concepts in experimental physics. Crucial are the multifarious roles of the reaction medium, understood as the solvent and protein frames of metalloprotein ET centres. Molecular charge transfer theory has a broadly established basis but offers novel frames specific to interfacial (bio)electrochemical ET towards the nanoscale and single-molecule levels. We shall discuss this in the context of electrochemical *in situ* STM of single-molecule redox activity. Theoretical aspects associated with electrochemical SET, and molecular electronics such as molecular rectification or amplification, are emerging as other novel elements of molecular charge transfer theory [29–32].

In contrast to *in situ* AFM in aqueous media, *in situ* STM (also denoted as '*operando*' STM) differs both technologically and conceptually from STM in vacuum or air. Both substrate and tip must be subjected to electrochemical potential control, in order to suppress spurious Faradaic currents, and the tip must be insulated so that only the outermost microscopic part is exposed. The *conceptual* differences can be illustrated by comparison between interfacial electrochemical ET at the semi-infinite electrochemical electrode–solution interface and the *in situ* STM redox process in the tunnelling gap between the enclosing substrate and tip.

The electrochemical, say cathodic current, $j(\eta)$, at the overpotential η, is [24, 25]

$$j(\eta) = \int \mathrm{d}\varepsilon\, f(\varepsilon)\rho(\varepsilon)i(\varepsilon;\eta); \qquad i(\varepsilon;\eta) = eC_{ox}(z^*)\Delta z W(\varepsilon;\eta). \tag{1}$$

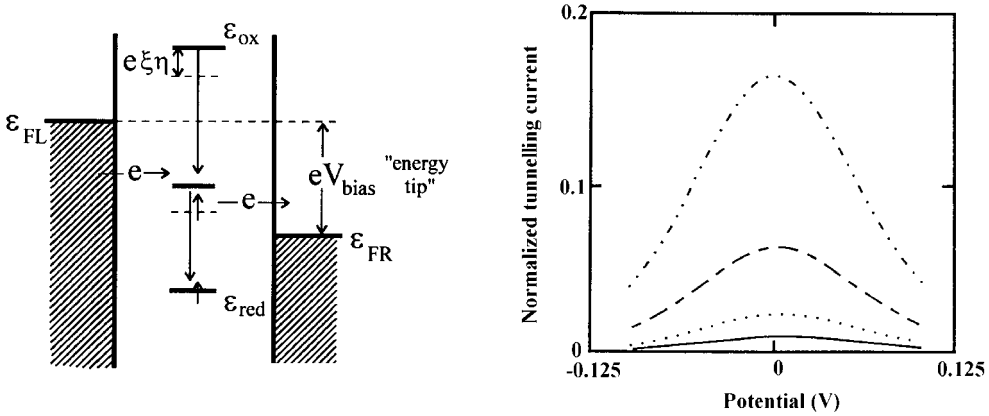

Figure 1. Left: electronic energy diagram of *in situ* STM of a redox molecule. Tunnelling from the negatively (substrate, left) to the positively (tip, right) biased electrode via the molecular redox level. This level is initially vacant (oxidized). *Fluctuations* in the environmental nuclear configurations take the vacant level close to the substrate Fermi level where the first ET step occurs. The occupied level then relaxes vibrationally towards equilibrium in the reduced state, transmitting coherently a (large) number of electrons. The reduced level is trapped below the tip Fermi level when the bias voltage is small. Renewed thermal activation induces ET from the occupied redox level to the tip. When the bias voltage is large the equilibrated reduced level remains *above* the tip Fermi level and multi-ET continues. Right: 'spectroscopic' relations between the normalized *in situ* STM tunnelling current, $i_{tunn}^{adiab}/i_{tunn}^{adiab,\max}$, and the substrate overpotential. The maximum is at the equilibrium substrate potential when the bias voltage distribution in the tunnelling gap is symmetric ($\gamma = 1/2$). Increasing currents correspond to $E_r = 8$, 12, 16 and 20. Energy quantities in units of k_BT.

$j(\eta)$ is carried by all the electronic levels of energy, ε in the electrode. $f(\varepsilon)$ is the Fermi function, $\rho(\varepsilon)$ the level density, e the electronic charge, $C_{ox}(z^*)$ the oxidized adsorbate redox level concentration at the distance z^* from the electrode and Δz a narrow z-range around z^*. The rate constant $W(\varepsilon;\eta)$ (s^{-1}) holds all information about nuclear reorganization, overpotential dependence and electron tunnelling. We shall use the broadly valid form [24, 25, 49, 50]

$$W(\varepsilon;\eta) = \kappa_{el}\frac{\omega_{eff}}{2\pi}\exp\left\{-\frac{[E_r + e\eta - (\varepsilon - \varepsilon_F)]^2}{4E_r k_B T}\right\} \tag{2}$$

where E_r is the nuclear reorganization Gibbs free energy, ω_{eff} the effective vibrational frequency, ε_F the Fermi energy, k_B Boltzmann's constant, T the temperature and κ_{el} $(\varepsilon;\eta)$ the electronic transmission coefficient (tunnelling factor). In the diabatic limit of weak interaction between the redox molecule and the electrode $\kappa_{el}(\varepsilon;\eta)k_BT \ll 1$ and tunnelling features are directly apparent. In the opposite, adiabatic limit κ_{el} $(\varepsilon;\eta)k_BT \to 1$ and tunnelling appears only indirectly.

Figure 1 illustrates *in situ* STM of a molecular redox adsorbate [30, 31]. The level can exist in an oxidized, ε_{ox}, and a reduced valence state, ε_{red}. Due to strong interaction with the environment the oxidized state has a significantly higher energy than the reduced state *at equilibrium*. Nuclear configurational *fluctuations* take the level to regions where electrons can be accepted from the negatively (from here on, substrate) and donated to the positively biased electrode (from here on, tip). *In situ* STM thus *resembles* electrochemical ET but the following *differences* are crucial.

(1) The *first* difference arises at small bias voltage, $|eV_{bias}| < E_r$. After the first ET step, from substrate to molecule, only a narrow $|eV_{bias}|$-range ('energy tip') is available for

electron transmission to the tip. As the overpotential is increased the current first rises but drops again as the reduced level is temporarily trapped below both Fermi levels. Renewed thermal activation is, next, needed for the second step. A spectroscopic feature thus arises in the current/overpotential and current/bias voltage correlations, in contrast to electrochemical ET where the current rise is followed by a wide plateau of constant current.

(2) A *second* difference is that as the temporarily occupied redox level is taken across the energy tip, i.e. the energy region between the Fermi levels of the negatively (left, ε_{FL}) and positively (right, ε_{FR}) biased electrode, a new ET phenomenon arises. When the electrode–molecule interactions are strong, a *multitude* of electrons, up to two orders of magnitude, are transferred coherently before the occupied redox level is trapped below the Fermi levels. The current rise in the 'energy tip' region can thus be much stronger than for single ET.

(3) A *third* difference is that the nuclear reorganization energy in the tunnelling gap is significantly smaller than in the semi-infinite solvent space of electrochemical ET. This has implications, say for biological macromolecules for which significant bias voltages are mostly needed [51]. When $|eV_{bias}| > E_r$ the temporarily reduced redox level is no longer trapped *below* the tip Fermi level but in the 'energy tip' region *between* the two Fermi levels. The redox level therefore continues to transmit electrons, and the current only drops after further overpotential increase, cf below. The *character* of the *in situ* STM process for bias voltages, e.g. significantly in excess of 0.1 V, thus involves coherent multi-ET independent of the overpotential, in striking contrast to thermally activated ET processes at a single electrode–solution interface.

The following theoretical notions illuminate other aspects of *in situ* STM and single-molecule interfacial ET. A tunnelling current form, broadly valid in the adiabatic limit, is [31]

$$i_{tunn}^{adiab} = 2en_{o/r}\frac{k^{o/r}k^{r/o}}{k^{o/r}+k^{r/o}} \tag{3}$$

where $k^{o/r}$ and $k^{r/o}$ are the rate constants for reduction and oxidation, respectively. $k^{o/r}$ and $k^{r/o}$ follow patterns for electrochemical ET [24, 25]

$$\begin{aligned} k^{o/r} &= \frac{\omega_{eff}}{2\pi}\exp\left[-\frac{(E_r - e\xi\eta - e\gamma V_{bias})^2}{4E_r k_B T}\right]; \\ k^{r/o} &= \frac{\omega_{eff}}{2\pi}\exp\left\{-\frac{[E_r + e\xi\eta - (1-\gamma)eV_{bias}]^2}{4E_r k_B T}\right\} \end{aligned} \tag{4}$$

where ξ and γ are the fractions of the overpotential (ξ) and bias voltage (γ) at the redox site. $n^{o/r}$ is the *number* of electrons transmitted whilst the redox level relaxes through the energy tip

$$n_{o/r} = \frac{eV_{bias}}{\Delta\varepsilon}; \qquad \Delta\varepsilon \approx \frac{1}{\kappa_{el}^{L}\rho_L} + \frac{1}{\kappa_{el}^{R}\rho_R} \ll k_B T. \tag{5}$$

The indices 'L' (left) and 'R' (right) refer to the substrate and tip, respectively. Since, in the adiabatic limit, $\Delta\varepsilon \ll k_B T$, $n^{o/r} \gg 1$. From equation (5) the electronic transmission coefficients in the pre-exponential factor of equations (3) and (4) thus determine the *number* of electrons transmitted and not directly the tunnelling features such as in the diabatic limit of *weak* electrode–molecule interactions. An equivalent form of equations (3) and (4) is

$$i_{tunn}^{adiab} = \frac{1}{2}\rho\kappa_{el}(eV_{bias})\frac{\omega_{eff}}{2\pi}\exp\left(-\frac{E_r - eV_{bias}}{4k_B T}\right)\cosh^{-1}\left[\frac{(\frac{1}{2}-\gamma)eV_{bias} - e\xi\eta}{2k_B T}\right] \tag{6}$$

where $\rho\kappa_{el} \approx \rho_L\kappa_{el}^L \approx \rho_R\kappa_{el}^R$. This gives a tunnelling current *maximum* determined by the following simple relation between η and V_{bias}:

$$\eta = \eta_{\max} = \frac{1}{\xi}\left(\frac{1}{2} - \gamma\right)V_{bias}. \tag{7}$$

The maximum is at $\eta_{max} = 0$, i.e. at the equilibrium electrochemical potential, when the redox site is exposed to half the bias voltage, $\gamma = 1/2$, figure 1(B).

The tunnelling current at large bias voltages, cf above, is [51]

$$i_{tunn}^{adiab} = \frac{e}{\tau}\frac{1}{\{1 + \exp[\frac{\langle n\rangle(1-\langle n\rangle)E_r - \langle n\rangle(e\xi\eta + e\gamma V_{bias})}{k_BT}]\}}. \tag{8}$$

$\tau \approx \hbar/\Delta_M$ ($M = L$, R) is the electron exchange time for redox level broadening by electronic coupling with the substrate and tip. $\langle n\rangle$ is the average redox level population, taken as approximately constant in the 'energy tip' region. Equation (8) shows that the vacant redox level is again located *above* the *substrate* Fermi level at small η. As η is increased the current rises and the level is brought to traverse this Fermi level. As the occupied level, however, remains above the *tip* Fermi level the tunnelling current remains at a constant high value, transmitting a large number of electrons. The current only drops when the overpotential is increased further, to

$$e\xi\eta > eV_{bias}(1 - \gamma) - E_r \tag{9}$$

and the occupied redox level is trapped below the tip Fermi level.

Redox metalloproteins and other molecules where the redox centre is enveloped in bulky ligand matter broadly need bias voltages, which are, in the present context, large for stable imaging. An implication is, then, that the tunnelling pattern broadly imaged would correspond to the overpotential range $E_r > e\xi\eta > eV_{bias}(1 - \gamma) - E_r$, with both the vacant and occupied redox levels between the two Fermi levels, where coherent multi-ET prevails. Outside this range the currents are thermally activated and too small for reliable monitoring. This observation is important in interfacial ET strategies towards the nanoscale and single-molecule levels.

3. Metalloproteins and oligonucleotides in nanoscale *in situ* function

We discuss here nanoscale perspectives associated with redox protein and oligonucleotide monolayer electrochemistry on atomically planar electrodes, supported by other surface physics data, and *in situ* STM. Such an approach is novel in bioelectrochemistry.

3.1. Chemically modified Au(111) electrodes

Compatibility between proteins and the electrode surface is crucial for protein structural and functional integrity in the immobilized state. Electrode surface modification is frequently achieved by using promoter molecules. A thiol group links the promoter molecule to the Au surface, and a suitable functional group in the promoter molecule contacts the protein. The latter group can be hydrophobic, hydrophilic, electrically charged or neutral depending on the protein surface. The structure and other properties of modified Au(111) surfaces directly in aqueous buffer are illustrated in figures 2 and 3. Figure 2 shows high-resolution *in situ* STM of *n*-butanethiol (left) [52] and mercaptopropionic acid (MPA, right) [53]. Butanethiol packs in a $(2\sqrt{3} \times 3)$R30° lattice with four molecules per unit cell and constitutes a hydrophobic surface suitable for protein adsorption via hydrophobic surface patches. MPA forms instead a network of clusters of *six* individual MPA molecules connected via hydrogen bonds and

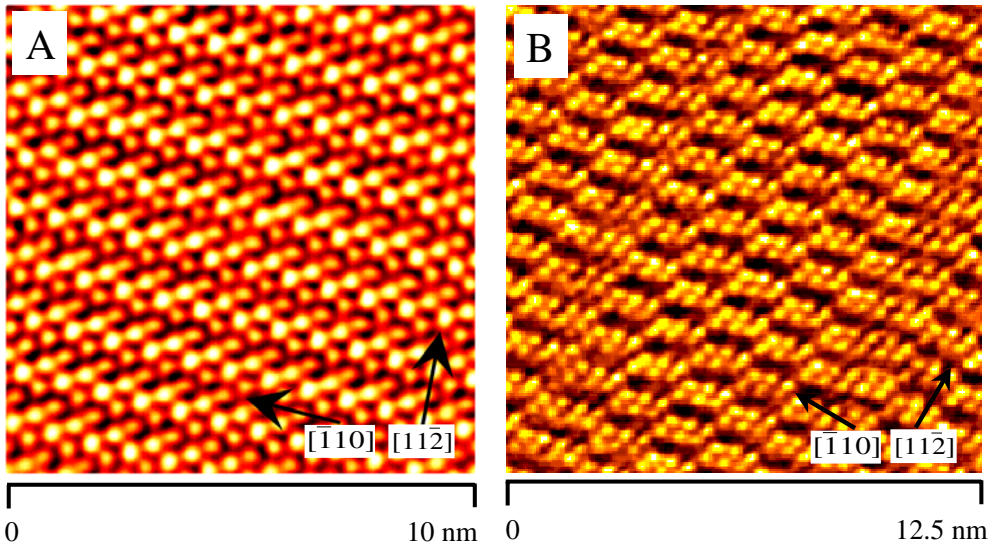

Figure 2. Left: *in situ* STM image of *n*-butanethiol on Au(111). 50 mM ammonium acetate $+3 \times 10^{-6}$ M *n*-butanethiol, pH 4.6. Scan area 10×10 nm^2. Working electrode potential: 0.05 V (SCE). Bias voltage 0.2 V. Tunnelling current 0.8 nA. W tip. Right: *in situ* STM image of mercaptopropionic acid on Au(111). 5 mM phosphate buffer, pH 7.9. Scan area 12×12 nm^2. Working electrode potential -0.15 V (SCE). Bias voltage -0.10 V. Tunnelling current 0.25 nA. Pt/Ir tip.

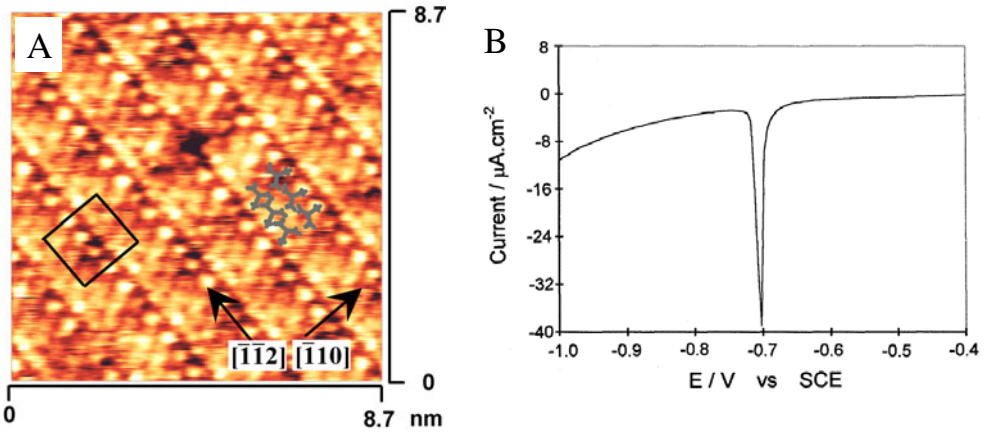

Figure 3. Left: *in situ* STM image of cystine on Au(111). 50 mM ammonium acetate $+1 \times 10^{-5}$ M cystine, pH 4.6. Scan area 8.7×8.7 nm^2. Working electrode potential: 0.1 V (SCE). Bias voltage: 0.2 V. Tunnelling current 0.8 nA. W tip. Right: linear scan voltammogram of cystine adsorbed on Au(111). 0.1 M NaOH, pH 13. Scan rate 10 mV s^{-1}.

water molecules. Figure 3, left, shows a high-resolution *in situ* STM image of the amino acid cystine (cysteine dimer). Highly ordered cluster networks are again apparent, organized in a $(3\sqrt{3} \times 6)$R30° lattice [52], with three cystine molecules in each cluster, suitable for adsorption of hydrophilic proteins. Figure 3, right, shows a linear scan voltammogram of cystine adsorbed on Au(111) in the reductive desorption region. A sharp peak at -705 mV (SCE) both provides

important information about the Faradaic charge, i.e. the surface coverage, crucial in STM assignments, and testifies to the high structural order of the monolayer.

Monolayers of butanethiol, MPA and cystine or cysteine are all suitable for gentle contacts between Au(111)-electrode surfaces and immobilized functional redox proteins in well defined orientations. Images such as in figures 2 and 3 offer first-hand high-resolution insight into the immediate molecular environment of functional redox metalloproteins and metalloenzymes on atomically planar electrochemical surfaces.

3.2. Functional redox metalloproteins on modified Au(111) electrodes

Several redox proteins adsorbed in monolayers on pure and modified Au(111) electrodes have recently been studied comprehensively. *In situ* STM under full potential control has, moreover, provided both structural features with single-molecule resolution, and electrochemical potential windows for functional monolayer stability. Proteins for which comprehensive characterization in this sense is available include *Pseudomonas aeruginosa* azurin (blue single-copper protein) [21, 22, 54], *Saccharomyces cerevisiae* cytochrome *c* (single-haem protein) [55], *Pyrococcus furiosus* ferredoxin (single Fe_3S_4-cluster) [53] and a synthetic 4-α-helix bundle carboprotein [19]. We address specifically *P. aeruginosa* azurin and *S. cerevisiae* cyt *c*.

3.2.1. Single-molecule structure, organization and functional control of P. aeruginosa azurin on pure and modified Au(111) surfaces. Studies of *P. aeruginosa* azurin have disclosed high structural detail and functional control of a surface-immobilized redox metalloprotein. The studies have shown a need for *comprehensive* approaches based both on electrochemistry and other state-of-the-art surface technology, and perspectives and limitations in the *in situ* STM approach [6, 21, 22, 51].

Figure 4 shows the three-dimensional structure of azurin with two structural elements highlighted, i.e. the Cu-redox centre with the His/Cys/Met/Gly ligand sphere, and the surface disulfide group. Hydrophobic residues, enabling facile electron exchange with solute reaction partners or hydrophobic electrode surfaces, dominate the protein surface around the copper centre. Azurin forms well defined stable monolayers on alkanethiol monolayers self-assembled on Au surfaces, with the copper centre facing the electrode (figure 4). The surface disulfide group, on the opposite side of the protein, is suitable for direct linking of azurin to the Au(111) surface. The overall protein structure is robust enough that functional integrity is retained in the adsorbed state. The two functional units are linked by β-strands, facilitating ET also *through* the protein.

The studies have provided the following coherent view of azurin monolayer dynamics important in metalloprotein function at the nanoscale and single-molecule levels: [20–22].

(1) Interfacial capacitance data and linear scan voltammetry of azurin on bare single-crystal Au(111) electrodes in the reductive desorption region point to azurin adsorption via the disulfide group. This is supported by 163.3/162.2 eV S_{2p} and 164.1 eV sulfur Cu-ligand signals in XPS.
(2) *In situ* STM discloses 70% azurin monolayer coverage on Au(111) at the isoelectric point (pH 4.6). Structural resolution is at the *single-molecule* level with molecular structures of the same lateral extension as in the crystallographic dimensions of azurin (3.7 ± 0.4 nm, figure 4). The monolayers are stable for weeks.
(3) ET functional integrity of azurin is retained in the adsorbed state, shown by symmetric cathodic and anodic differential pulse voltammetric signals in the $Cu^{2+/+}$ redox potential region (0.1 V versus SCE, figure 5). No signals appear for Zn-substituted azurin [20, 21].

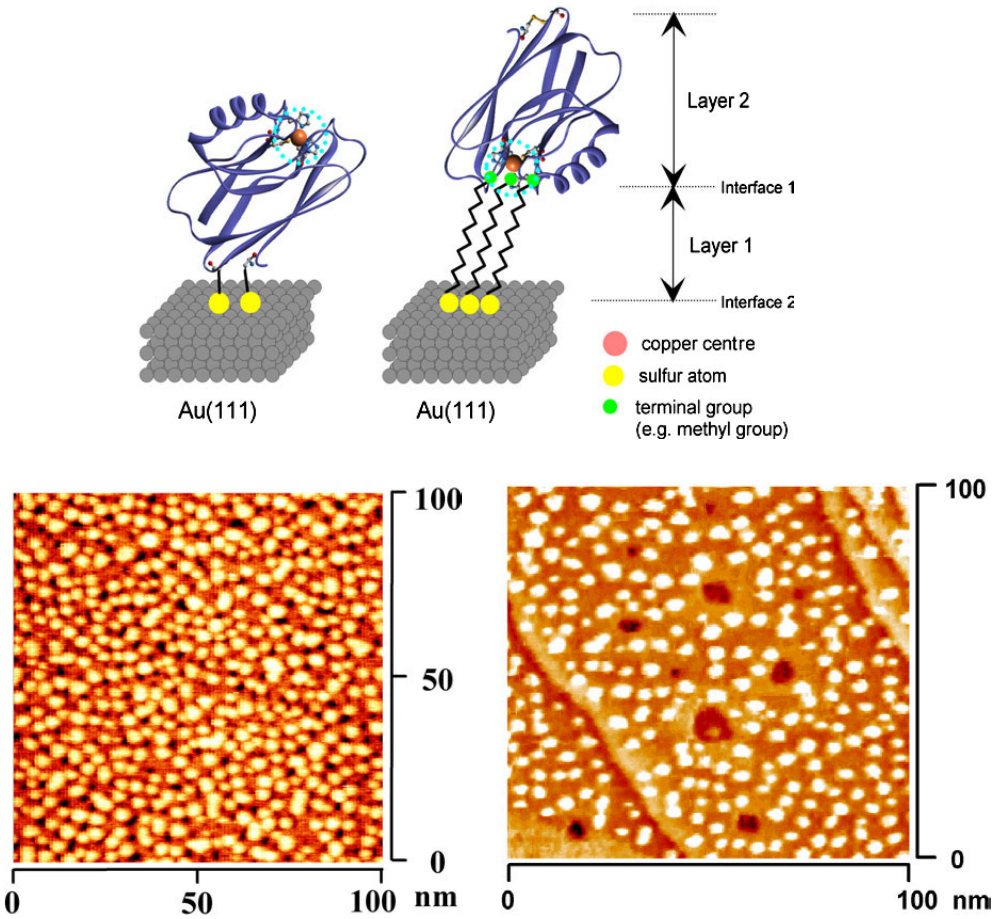

Figure 4. Top: three-dimensional structure of azurin and schematic views of azurin adsorption on bare Au(111) (left) and hydrophobic alkanethiol monolayers self-assembled on Au(111) (right). In the former orientation chemisorption is via protein disulfide with the copper centre opposite the Au(111) surface. The copper centre faces the surface in the latter orientation. Azurin structure from [56] and Protein Data Bank. Molscript Graphics [57]. Bottom, left: *in situ* STM image of functional *P. aeruginosa* azurin on bare Au(111). 50 mM ammonium acetate, pH 4.6. Scan area 100 × 100 nm^2. Substrate potential: −0.1 V (SCE). Bias voltage: 0.2 V. Tunnelling current 0.8 nA. W tip [21]. Bottom, right: *ex situ* STM image of *P. aeruginosa* azurin on decanethiol self-assembled on Au(111). Scan area 100 × 100 nm^2. Prepared from 5 mM ammonium acetate, pH 4.6. Bias voltage 0.81 V. Tunnelling current 0.16 nA. W tip [22].

Such observations show that stable, functional dense azurin monolayers bound directly to Au(111) via protein surface disulfide self-assemble spontaneously. The monolayers can be mapped with single-molecule resolution, but long-range lateral order has not been achieved.

The following other details about azurin behaviour on bare Au(111) have emerged [51]:

(4) The azurin layer is stable in the electrochemical potential range from −0.4 to +0.3 V (SCE) in the semi-infinite *electrochemical* configuration, and desorbs reductively and oxidatively, respectively, at these two boundaries. The *in situ* STM stability range is narrower and confined to substrate potentials from −0.35 to 0 V (SCE) at a bias voltage

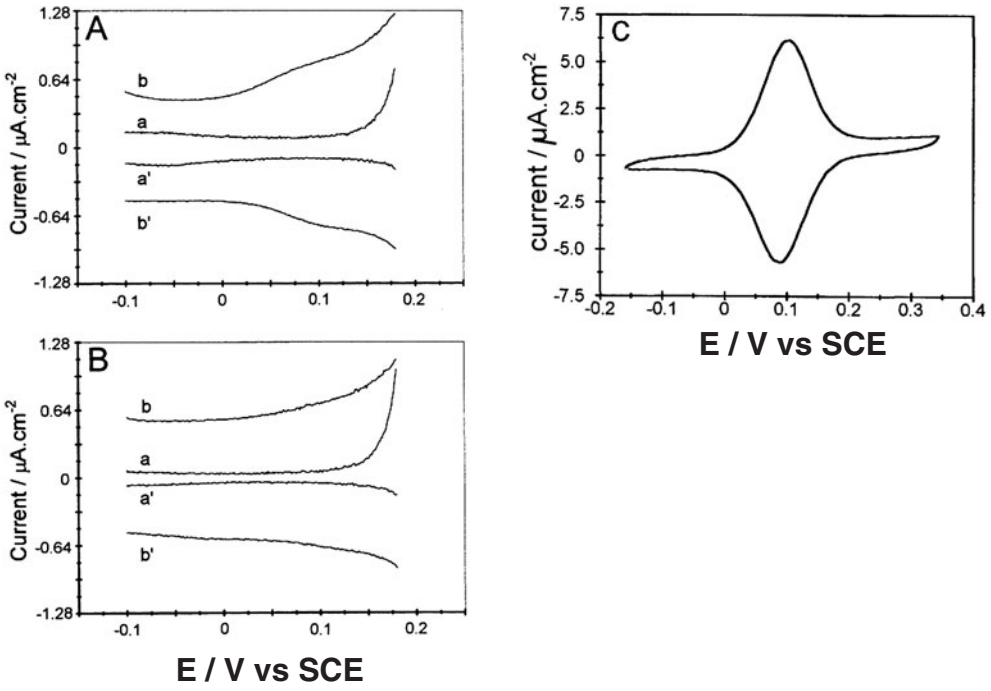

Figure 5. Monolayer differential pulse voltammograms of azurin (A) and Zn-substituted azurin (B) on Au(111) [20, 21]. 50 mM ammonium acetate, pH 4.6. Azurin concentrations in curves a and a*, zero; in curves *b* and *b*′, 1.5×10^{-7} M. (C) Monolayer linear scan voltammograms of azurin on dodecanethiol monolayer self-assembled on Au(111). 50 mM ammonium acetate, pH 4.6. Scan rate 2 V s^{-1} [22].

of 0.2 V. The *in situ* STM contrast (representative of the tunnelling current) is, moreover, independent of the overpotential in this range. The constant image contrast accords with the theoretical notion of coherent multi-ET and the accommodation of both the oxidized and reduced redox levels in the 'energy tip' region over a significant overpotential range [51], cf section 2.3 and equations (8) and (9). The narrower stability range is likely to be caused by field and mechanical tip effects, but the contrast decay at the positive stability boundary can *also* be caused by redox-induced tunnelling mechanisms (section 2), as this boundary is close to the $Cu^{2+/+}$ equilibrium potential [51].

The ET patterns change drastically in the alternative adsorption mode, where azurin is adsorbed on the hydrophobic surface of variable-length alkanethiols self-assembled on Au(111). The strong hydrophobic interactions fix azurin in a well defined orientation with the copper centre facing the electrode. The most striking difference from *chemisorption* of azurin directly on Au(111) is that robust, almost ideal monolayer voltammetry emerges. This would apply generally for well defined functional protein and enzyme monolayer formation. The following observations disclose other important features of azurin behaviour on the modified Au(111) surfaces [22].

(a) Azurin adsorbs in stable monolayers with uniform coverage (figure 4).
(b) Almost ideal azurin monolayer voltammetry emerges. Interfacial electron tunnelling between the electrode and the copper centre is significantly faster than in the direct adsorption mode through the protein, for similar tunnelling distances.

(c) Azurin monolayer voltammetry is stable and sensitive, with voltammetric signals even for less than 2% azurin coverage.

The following detailed ET dynamics emerges from azurin monolayer voltammetry at long (nine to 18 carbon atoms) alkanethiols.

(d) The voltammetric peaks separate, indicative of *kinetic* interfacial ET control. The standard rate constants, at $\eta = 0$, follow an exponential distance relation, strongly reflecting interfacial electron tunnelling across the alkanethiol.
(e) The overpotential dependence of the cathodic and anodic rate constants is symmetric and follows a quadratic dependence. The nuclear reorganization Gibbs free energy is $\approx$0.3 eV, according with expectations for the apolar interfacial microenvironment.

The totality of data suggests, first, that azurin is a 'prototype' redox protein for functional monolayer formation, with features of high structural order, stability and sensitivity. Azurin follows, further, theoretical expectations regarding interfacial tunnelling and overpotential patterns. *Molecular* structural resolution has, finally, been achieved and disclosed novel details in single-molecule interfacial ET. All this is generally important in single-molecule redox protein mapping and control, once the microenvironments have been identified and characterized.

Other perspectives along these lines have emerged for *P. furiosus* ferredoxin [53] and *S. cerevisiae* cyt *c* [55]. We proceed to a discussion of the latter redox metalloprotein.

3.2.2. Single-molecule structure and function of S. cerevisiae cyt c on Au(111) surfaces. The small redox haem group protein, horse heart cytochrome *c* (HHC), was the first redox metalloprotein brought to display diffusion-controlled cyclic voltammetry [58] mediated by hydrogen bond contacts between the protein and adsorbed monolayers of 4,4′-bipy or 1,2-4,4′-bipy-disulfide on polycrystalline Au electrodes. HHC also forms functional monolayers on ω-mercapto-carboxylates self-assembled on Au [59, 60]. In either case positively charged amino acid residues (lysines) around the exposed haem group edge are crucial in establishing gentle hydrogen-bonding or electrostatic contact between the metalloprotein and the self-assembled promoter monolayers on the electrode surface.

S. cerevisiae cytochrome *c* (YCC, figure 6) resembles HHC in the electrostatic charge distribution and the haem group orientation in the protein. YCC displays diffusion controlled voltammetry on poly- and single-crystal Au electrodes modified similarly as for HHC [55]. YCC also possesses a thiol group, from Cys102, close to the protein surface and moderately remote from the haem group (Fe–S distance 11.2 Å) [61]. The thiol group offers a link to the Au surface in an orientation reminiscent of azurin but surface immobilization is less stable as full thiol exposure requires some conformational reorganization. The secondary and tertiary structures of YCC are dominated by α-helices, while those of azurin are entirely dominated by β-strands. YCC therefore offers a target for comparison with azurin.

As for azurin, comprehensive data have provided a coherent view of YCC adsorption and ET dynamics on Au(111) electrodes. The molecule appears structurally and functionally more fragile than azurin but the behaviour of YCC substantiates that redox metalloproteins can be characterized to molecular resolution under conditions where protein function is retained. The following observations summarize the monolayer pattern on Au(111).

(1) As for azurin, YCC displays linear sweep and differential pulse voltammetry from *two* functional groups, i.e. the haem group and the chemisorbed thiolate group. The α-helix YCC structure is, however, less robust in the chemisorbed state than azurin, with a transient native haem group signal at +74 mV (SCE) (figure 6(B)) but a more robust signal at

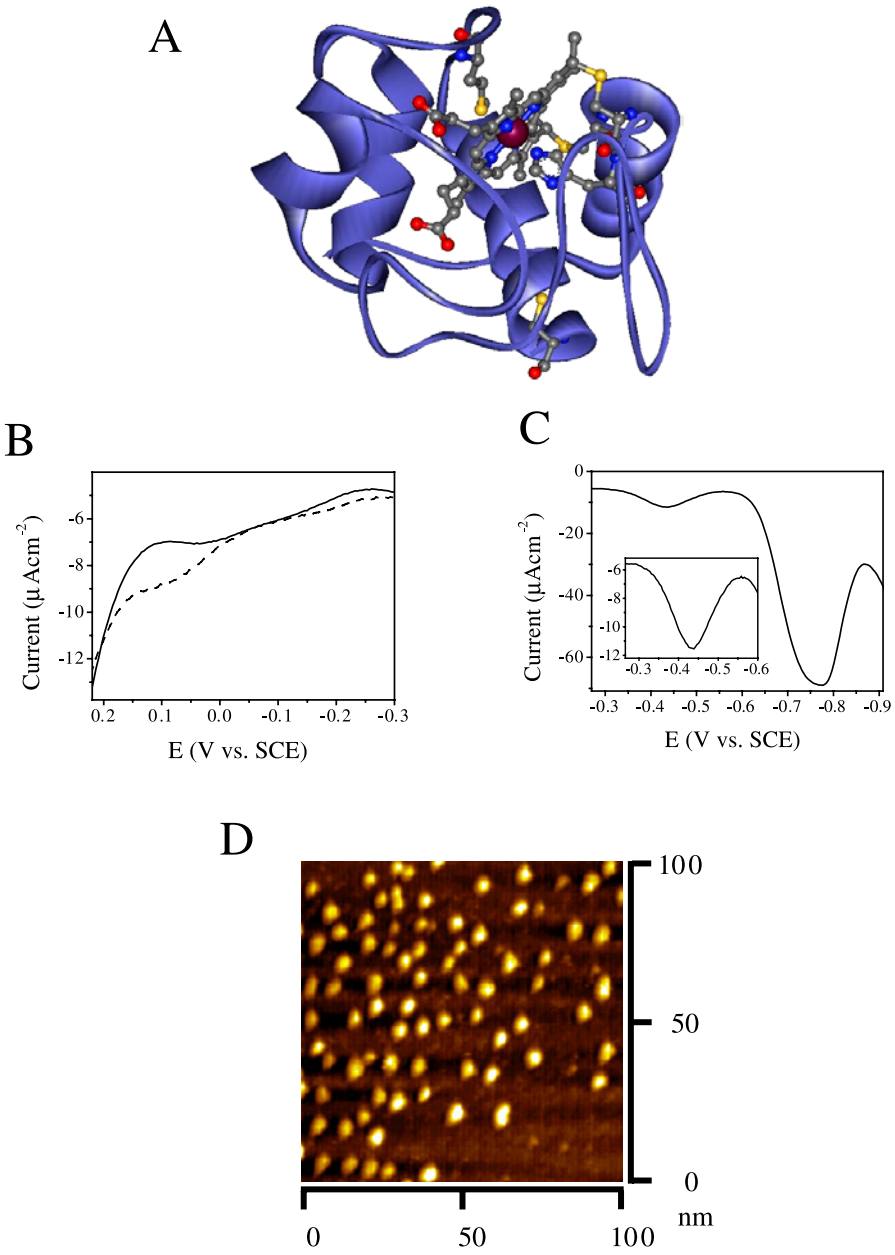

Figure 6. (A) Three-dimensional crystal structure of yeast cyt *c*. The haem group, the surface thiol group (Cys102) and the haem-linking thio-ethers are highlighted. Coordinates from [61] and Protein Data Bank. Molscript graphics [57]. (B) Differential pulse voltammograms of YCC reduction in the native haem group region (+0.200 V to −0.300 V (SCE). Dashed: 100 mM phosphate buffer, pH 7.3. Fully drawn: 100 mM $NaClO_4$. Scan rate 10 mV s^{-1}. (C) Differential pulse voltammogram covering the reductive desorption region and the region of non-natively ligated haem group reduction (−0.25 to −0.94 V (SCE)). 100 mM phosphate buffer, pH 7.3. Scan rate 10 mV s^{-1}. The strong signal at −0.73 V (SCE) represents reductive thiolate desorption, the weak signal at −0.43 V (SCE) the non-natively coordinated haem group. (D) *In situ* STM image of YCC on Au(111). 10 mM phosphate buffer, pH 7.5. Scan area 100 × 100 nm^2. Working electrode potential: −0.16 V (SCE). Bias voltage: −0.2 V. Tunnelling current 0.5 nA. W tip [55].

−440 mV (SCE) (figure 6). The latter can be assigned to a haem group in which the native axial methionine ligand has been replaced by a non-native ligand.

(2) XPS gives strong double-peak (163.3/162.2 eV) S_{2p} signals for YCC on Au(111). However, cytochromes unfold extensively in the ultrahigh-vacuum environment of XPS [62], exposing other S-residues than Cys102. A sulfur signal is therefore inconclusive as to the adsorption mode of YCC in aqueous buffer. HHC with no exposed thiol group thus gives a similar XPS pattern [55].

(3) Pre-fabricated microcantilevers of the same type as in AFM have become broadly available as substrates for MCS technology in microscale chemical analysis [63]. The merit of MCS technology is that the MCS responds broadly to (bio)molecular adsorption by adsorption-induced deflection detectable as changes in the cantilever mass, temperature or surface stress [63]. Biomolecular adsorption processes can also be followed in real time.
Adsorption of cysteine and YCC on Au-coated Si_3N_4 cantilevers from aqueous buffer has been followed by a novel MCS mode in which the Au-coated probe was combined with an uncoated reference cantilever [55]. MCS signals from non-specific adsorption can be subtracted in this way, leaving stress signals solely from specific adsorption via Au–S bond formation. MCS data have disclosed that both cysteine and YCC adsorption are accompanied by significant *tensile* surface stress, i.e. the adsorption forces the cantilever to bend upwards (the Au-coated side concave) due to attractive forces between the adsorbed molecules. Several adsorption phases, in ranges from $<10^2$ s to $>10^3$, can be distinguished and assigned to different collective surface processes. These observations add important features to the view of YCC and cysteine adsorption.

(4) As for azurin, *in situ* STM of YCC on Au(111) in aqueous buffer illuminates both merits and limitations of this approach. Figure 6(D) shows a representative image. Structures of molecular lateral extension close to that of YCC (≈4 nm) are clearly visible, with the following other observations.

  (i) The surface population is significantly smaller (≈15%) than for azurin (≈70%).
  (ii) Imaging is robust in the electrochemical potential range from −0.4 to −0.2 V (SCE), with bias voltages from −0.1 to –0.2 V where the native haem group is in the reduced state. The redox level of the non-native haem group, with a much lower reduction potential (figures 6(B) and (C)), is, however, *between* the two Fermi levels in the electrochemical substrate potential range, i.e. in the 'energy tip' region where fast coherent multi-ET via this level is feasible, cf above.
  (iii) Significant adsorbate depopulation is seen outside the potential ranges of robust imaging. The depopulation process can be controlled to an extent that patterns in the YCC monolayers can be created. This offers a possible biotechnological perspective [55].

As for azurin, *in situ* STM of YCC thus offers a single-molecule view of YCC organization and function on Au(111). The electrochemical potential ranges of robust imaging suggest that, as for azurin, coherent multi-ET, here mediated by the haem group in a *non-native* ligand state, could be a valid view of the tunnelling mechanism of YCC.

3.3. In situ oligonucleotide dynamics on Au(111)

The comprehensive approach to adsorbed redox metalloproteins on well characterized metallic surfaces in contact with aqueous buffer, based particularly on electrochemistry, spectroscopy and *in situ* STM, also applies to variable-composition oligonucleotides. These can be immobilized in monolayers on Au(111)-electrode surfaces via covalently attached thiol

linkers, and mapped in detail [64]. Single-molecule *in situ* STM mapping holds at least two perspectives. One is the base-pair specific electronic conduction of DNA, currently in intense focus [65–67], which could also be addressed by *in situ* STM. The other perspective is to map the *hybridization* of immobilized single-strand oligonucleotides with complementary single strands in the aqueous buffer, leading ultimately towards single-molecule biological screening.

Figure 7 shows features of short oligonucleotide immobilization on Au(111). The molecule is a sequence of ten A–T base pairs (A = adenine, T = thymine) (figure 7, top). Double strands at this length are stable in bulk solution. The 10-A–T sequence is immobilized via a ω-hexanethiol linker attached to the 5′-end of the A strand. Figure 7(B) shows a strong reductive desorption signal at −720 mV (SCE) corresponding roughly to monolayer coverage. Figure 7(C) shows an *in situ* STM image of thiolated 10-A–T on Au(111). High coverage of single-molecule structures as well as a large number of pits in the surface, caused by chemical interaction between the thiol linker and the Au surface, are apparent. Such data show that the combined single-crystal electrochemistry and *in situ* STM approach offers similar perspectives for oligonucleotides as for redox metalloproteins. The molecular conduction mechanism is currently more elusive than for redox proteins but can be approached once systematic variable-sequence data are available.

4. Concluding remarks

Adsorption of proteins on electrodes and other surfaces is often undesirable due to surface blocking, but has come to offer perspectives in chemical and biological sensing based on subtle interactions between the biomolecules, the metallic electrode, and analyte substrates in solution. Novel features are that biotechnology extending to protein production, modification (site-directed mutagenesis) and wiring can be combined with state-of-the-art physical techniques. We have focused on physical electrochemistry, particularly single-crystal, atomically planar electrode surfaces, and *in situ* STM. This has led to the notion of truly well characterized electrochemical surfaces, and bioelectrochemical sciences towards nanoscale and single-molecule levels.

We have illuminated these perspectives by two specific redox metalloproteins and a short double-strand oligonucleotide, immobilized on Au(111) surfaces in contact with aqueous buffer. Comprehensive data have pointed to coherent views of protein or oligonucleotide adsorption in well defined orientations on the surface and, for the proteins, with interfacial ET function retained. The perspectives of *in situ* STM have extended to structural mapping and visualization of redox proteins in direct action at the single-molecule level, and disclosed novel ET mechanisms based on coherent, activationless multi-ET through the metalloproteins. Such notions may also apply to electronic conduction in oligonucleotides.

The novel area of nanoscale bioelectrochemistry at ‘clean’ surfaces holds exciting perspectives for mapping (bio)molecular electronic reactivity, functional individuality (stochastic features), chemical reactivity etc, at the single-molecule level. In due course technological hybrid-molecular device function in chemical and biological sensing, multi-sensor monolayer and single-molecule arrays, supramolecular pattern formation and biological screening in general can be envisaged.

Acknowledgments

Financial support from the Danish Technical Science Research Council (contract no 26-00-0034) and the EU Programme INTAS (contract no 99-1093) is acknowledged. This work was

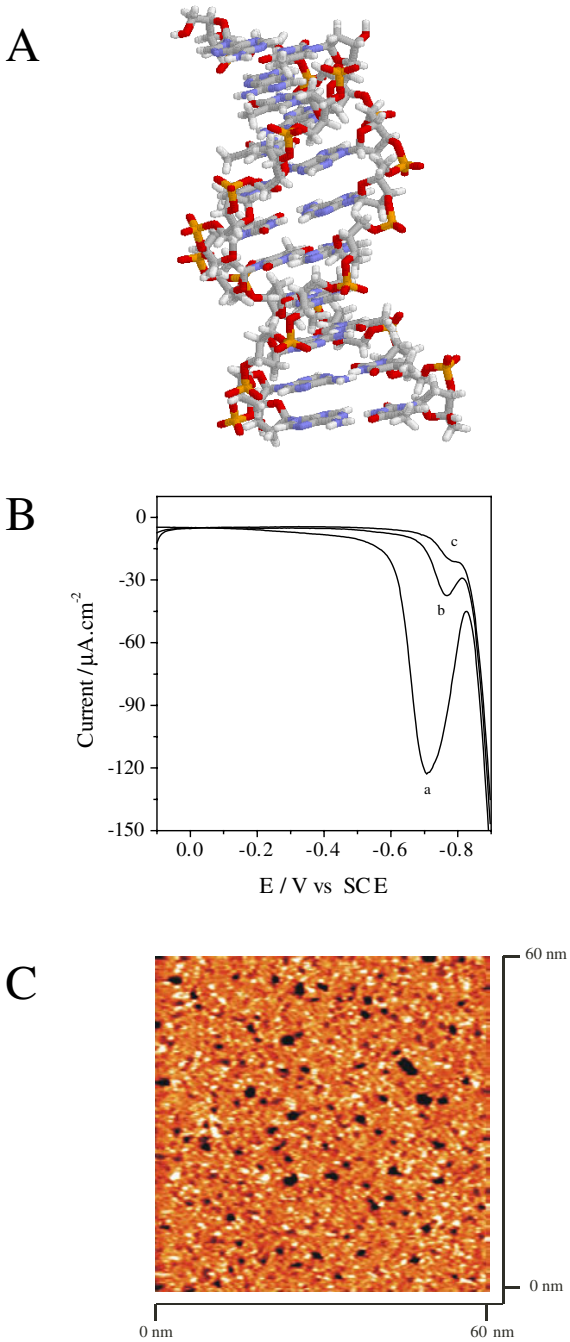

Figure 7. (A) Three-dimensional structure of oligonucleotide double strand with a sequence of ten A–T base pairs. Graphics from [68]. The hexanethiol linker not shown. (B) Differential pulse voltammogram of thiolated 10-A–T on Au(111). (a) First scan. (b) Second scan. (c) Third scan. 100 mM phosphate buffer, pH 6.9. Scan rate 10 mV s^{-1}. (C) *In situ* STM image of thiolated 10-A–T on Au(111). 10 mM phosphate, pH 6.8. Scan area 60 × 60 nm^2. Working electrode potential −0.45 V (SCE). Bias voltage −0.15 V. Tunnelling current 0.25 nA. W tip [64].

completed whilst one of us (JU) was on leave at the School of Chemistry, University of Sydney. The hospitality of the University of Sydney is acknowledged.

References

[1] Gilardi G and Fantuzzi A 2001 *Trends Biotechnol.* **19** 468
[2] Shipway A N and Willner I 2001 *Accounts Chem. Res.* **34** 421
[3] Armstrong F A and Wilson G S 2000 *Electrochim. Acta* **45** 2623
[4] Service R F 1998 *Science* **282** 396
[5] Chen L, Haushalter K A, Lieber C M and Verdine G L 2002 *Chem. Biol.* **9** 345 and references therein
[6] Zhang J, Chi Q, Kuznetsov A M, Hansen A G, Wackerbarth H, Christensen H E M, Andersen J E T and Ulstrup J 2002 *J. Phys. Chem.* B **106** 1131
[7] Fritz J, Baller M, Lang H P, Rothuizen H, Vettiger F, Meyer E, Güntherodt H-J, Gerber C and Gimzewski J K 2000 *Science* **288** 316
[8] Storm G and Crommelin D J A 1998 *Pharm. Sci. Technol. Today* **1** 19
[9] Telegdi J, Keresztes Z, Pálinkás G and Kálmán E 1998 *Appl. Phys.* **66** S639
[10] Telegdi J, Shaban A, Beczner J, Keresztes Z and Kálmán E 1998 *Mater. Sci. Forum* **289** 77
[11] Kasemo B 2002 *Surf. Sci.* **500** 656
[12] Tirell M, Kokkoli E and Biesalski M 2002 *Surf. Sci.* **500** 61
[13] Davis J J, Hill H A O and Bond A M 2000 *Coord. Chem. Rev.* **200** 411
[14] Hianek T (ed) 2002 *Proc. 16th Int. Symp. on Bioelectrochemistry and Bioenergetics; Bioelectrochemistry* **55** 1–181 (Special issues)
Hianek T (ed) 2002 *Bioelectrochemistry* **56** 1–236
[15] Armstrong F A 2002 *J. Chem. Soc. Dalton Trans.* 661
[16] Choma C T, Lear J D, Nelson M J, Dutton P L, Robertson D E and DeGrado W F 1994 *J. Am. Chem. Soc.* **116** 856
[17] Rau H K, DeJonge N and Haehnel W 2000 *Angew. Chem. Int. Edn* **39** 250
[18] Jensen K J and Barany G 2000 *J. Peptide Res.* **56** 3
[19] Brask J, Wackerbarth H, Jensen K J, Zhang J, Chorckendorff I and Ulstrup J 2003 *J. Am. Chem. Soc.* **125** 94
[20] Chi Q, Zhang J, Friis E P, Andersen J E T and Ulstrup J 1999 *Electrochem. Commun.* **1** 91
[21] Chi Q, Zhang J, Nielsen J U, Friis E P, Chorckendorff I, Canters G W, Andersen J E T and Ulstrup J 2000 *J. Am. Chem. Soc.* **122** 4047
[22] Chi Q, Zhang J, Andersen J E T and Ulstrup J 2000 *J. Phys. Chem.* B **105** 4669
[23] Contributions in
Jortner J and Ratner M (ed) 1997 *Molecular Electronics* (Oxford: Blackwell)
[24] Kuznetsov A M 1995 *Charge Transfer in Physics, Chemistry, and Biology* (Reading, MA: Gordon and Breach)
[25] Kuznetsov A M and Ulstrup J 1999 *Electron Transfer in Chemistry and Biology. An Introduction to the Theory* (Chichester: Wiley)
[26] Marcus R A and Sutin N 1985 *Biochim. Biophys. Acta* **811** 265
[27] Marcus R A 2000 *J. Electroanal. Chem.* **483** 2–6
[28] Han W, Durantini E N, Moore T A, Moore A L, Gust D, Leatherman G, Deely G R, Tao N and Lindsay S M 1997 *J. Phys. Chem.* **101** 10719
[29] Hansen A G, Wackerbarth H, Nielsen J U, Zhang J, Kuznetsov A M and Ulstrup J 2003 *Russ. J. Electrochem.* **39** 117
[30] Friis E P, Kharkats Yu I, Kuznetsov A M and Ulstrup J 1998 *J. Phys. Chem.* A **102** 7851
[31] Kuznetsov A M and Ulstrup J 2000 *J. Phys. Chem.* A **104** 11531
Kuznetsov A M and Ulstrup J 2001 *J. Phys. Chem.* **105** 7494 (erratum)
[32] Kuznetsov A M and Ulstrup J 2002 *J. Chem. Phys.* **116** 2149
[33] Avouris P 2002 *Chem. Phys.* **282** 429
[34] Ho P K H, Kim J-S, Burroughes J H, Becker H, Li S F Y, Brown T M, Cacialli F and Friend R H 2000 *Nature* **404** 481
[35] Balzani V, Credi A, Raymo F M and Stoddart J F 2000 *Angew. Chem. Int. Edn* **39** 3348
[36] Kolb D M, Ullman R and Will T 1997 *Science* **275** 1097
[37] Chi Q, Zhang J, Friis E P, Andersen J E T and Ulstrup J 2000 *Surf. Sci.* **463** L641
[38] Moerner W 2002 *J. Phys. Chem.* B **106** 910
[39] Contributions in
Mink J, Jalsovszky G and Keresztury G (ed) 2002 *Proc. 18th Int. Conf. on Raman Spectroscopy (Budapest)* (Chichester: Wiley)

[40] For a review, see [6]
[41] Radmacher M, Fritz M, Hansma H G and Hansma P K 1994 *Science* **265** 1577
[42] Kasas S, Thomson N H, Smith B L, Hansma H G, Zhu X, Guthold M B, Bustamentre C, Kool E T, Kashlev M and Hansma P K 1997 *Biochemistry* **36** 461
[43] Ha T, Ting A Y, Liang J, Caldwell W B, Deniz A A, Chela D S, Schulz P G and Weiss S 1999 *Proc. Natl Acad. Sci. USA* **96** 893
[44] Lu H P, Lun L and Xie X S 1998 *Science* **282** 1877
[45] Lu H P and Xie X S 1997 *J. Phys. Chem.* B **101** 2753
[46] Bard A J and Fan F-R F 1996 *Accounts Chem. Res.* **29** 572
[47] Fan F F and Bard A J 1997 *Science* **277** 1791
[48] Templeton A C, Wuelfing W P and Murray R W 2000 *Accounts Chem. Res.* **33** 27
[49] Dogonadze R R and Chizmadzhev Yu I 1962 *Dokl. Akad. Nauk SSSR, Ser. Fiz. Khim.* **144** 1077
[50] Dogonadze R R and Chizmadzhev Yu I 1962 *Dokl. Akad. Nauk SSSR, Ser. Fiz. Khim.* **145** 848
[51] Zhang J, Kuznetsov A M and Ulstrup J 2003 *J. Electroanal. Chem.* **511** 133
[52] Zhang J, Chi Q, Nielsen J U, Friis E P, Andersen J E T and Ulstrup J 2000 *Langmuir* **16** 7229
[53] Zhang J, Christensen H E M, Ooi B L and Ulstrup J 2003 submitted
[54] Friis E P, Andersen J E T, Madsen L L, Møller P and Ulstrup J 1997 *J. Electroanal. Chem.* **431** 35
[55] Hansen A G, Boisen A, Nielsen J U, Wackerbarth H, Chorckendorff I, Andersen J E T, Zhang J and Ulstrup J 2002 *Langmuir* **19** 3419
[56] Nar H, Messerschmidt A and Huber R 1991 *J. Mol. Biol.* **221** 765
[57] Kraulis P 1991 *J. Appl. Crystallogr.* **24** 946
[58] Eddowes M and Hill H A O 1979 *J. Am. Chem. Soc.* **101** 4461
[59] Song S, Clark R A, Bowden E F and Tarlov M J 1993 *J. Phys. Chem.* **97** 6564
[60] Avila A, Gregory G W, Niki K and Cotton T M 2000 *J. Phys. Chem.* B **104** 2759
[61] Louie G V and Brayer G V 1990 *J. Mol. Biol.* **214** 527
[62] Clemmer D E, Hudgins R R and Jarrold M F 1995 *J. Am. Chem. Soc.* **117** 10141
[63] Raiteri R, Grattarola M, Butt H-J and Skládal P 2001 *Sensors Actuators* B **79** 115
[64] Wackerbarth H, Hansen A G, Grubb M, Zhang J and Ulstrup J 2003 in preparation
[65] Egal D, Nitzan A, Davis W B, Wasiliewski M R and Ratner M A 2000 *J. Phys. Chem.* B **104** 3817
[66] Hess S, Götz W, Davis W B and Michel-Beyerle M E 2001 *J. Am. Chem. Soc.* **123** 10046
[67] Giese B and Biland A 2002 *Chem. Commun.* 667
[68] http://www.3icgeb.trieste.it/~dna/model.it.html